

## Joint Variability of Global Runoff and Global Sea Surface Temperatures

GREGORY J. McCABE

*U.S. Geological Survey, Denver, Colorado*

DAVID M. WOLOCK

*U.S. Geological Survey, Lawrence, Kansas*

(Manuscript received 18 June 2007, in final form 5 October 2007)

### ABSTRACT

Global land surface runoff and sea surface temperatures (SST) are analyzed to identify the primary modes of variability of these hydroclimatic data for the period 1905–2002. A monthly water-balance model first is used with global monthly temperature and precipitation data to compute time series of annual gridded runoff for the analysis period. The annual runoff time series data are combined with gridded annual sea surface temperature data, and the combined dataset is subjected to a principal components analysis (PCA) to identify the primary modes of variability. The first three components from the PCA explain 29% of the total variability in the combined runoff/SST dataset. The first component explains 15% of the total variance and primarily represents long-term trends in the data. The long-term trends in SSTs are evident as warming in all of the oceans. The associated long-term trends in runoff suggest increasing flows for parts of North America, South America, Eurasia, and Australia; decreasing runoff is most notable in western Africa. The second principal component explains 9% of the total variance and reflects variability of the El Niño–Southern Oscillation (ENSO) and its associated influence on global annual runoff patterns. The third component explains 5% of the total variance and indicates a response of global annual runoff to variability in North Atlantic SSTs. The association between runoff and North Atlantic SSTs may explain an apparent steplike change in runoff that occurred around 1970 for a number of continental regions.

### 1. Introduction

Interest in the effects of climate change on the hydrologic cycle has led to studies of observed hydroclimatic variables on a global scale. Dai et al. (1997), for example, identified two modes of variability in global precipitation for the period 1900–88. One mode indicated an El Niño–Southern Oscillation (ENSO)–related pattern and the second mode reflected a linear trend in global precipitation. The trends in precipitation were primarily increases in North America, mid- to high-latitude Eurasia, Argentina, and Australia. In another study, Dai et al. (2004) examined the variability of the global annual Palmer drought severity index (PDSI) values using principal components analysis. Similar to the study of global precipitation, Dai et al.

(2004) reported that the first two principal components of global annual PDSI are related to long-term trends and the ENSO. Decreasing PDSI values, indicating increasing drought, were especially apparent in the Sahel region of Africa and in high-latitude regions of North America and Asia, while increasing PDSI values were apparent in some midlatitude continental zones in both the Northern and Southern Hemispheres.

McCabe and Palecki (2006) used principal components analysis and singular value decomposition (SVD) to examine primary modes of global PDSI and sea surface temperature (SST) variability on decadal and multidecadal time scales during the period 1925–2003. Results indicated that two principal components explain approximately 38% of the variance in the detrended and smoothed PDSI data. The score time series and loadings of these two principal components indicated that the first mode of decadal-scale PDSI variability was related to the Pacific decadal oscillation (PDO) and Indian Ocean SSTs, while the second mode was correlated with the Atlantic multidecadal oscillation (AMO).

---

*Corresponding author address:* Gregory J. McCabe, U.S. Geological Survey, Denver Federal Center, MS 412, Denver, CO 80225.

E-mail: gmccabe@usgs.gov

In a number of studies, variability in SSTs has been shown to be a significant driving force of hydroclimate variability (Fontaine and Janicot 1996; Enfield and Alfaro 1999; Rodwell et al. 1999; Dettinger et al. 2000; Dettinger and Diaz 2000; Enfield et al. 2001; Nicholson et al. 2001; Giannini et al. 2003; Gray et al. 2003; Sutton and Hodson 2003; Hidalgo 2004; McCabe et al. 2004; Shabbar and Skinner 2004; Schubert et al. 2004; Seager et al. 2005; Sutton and Hodson 2005; McCabe and Paulecki 2006; Parker et al. 2007). These studies have shown the strong influence of tropical Pacific Ocean SSTs on hydroclimate across the globe. More recently, several of these studies also have shown substantial associations between North Atlantic SSTs and global hydroclimate, particularly on decadal to multidecadal time scales (Enfield et al. 2001; Hidalgo 2004; McCabe et al. 2004; Sutton and Hodson 2005; McCabe and Paulecki 2006; Parker et al. 2007).

The previously described studies have improved our understanding of linkages between ocean temperatures and continental climate. There still are significant gaps, however, in our knowledge of how SSTs affect continental streamflow on a global scale. Progress toward understanding the historical connections between global runoff and SSTs requires a spatially extensive streamflow dataset. A high-quality and spatially detailed streamflow dataset does not exist. Instead of using measured streamflow, the analysis presented in this paper relies on the  $0.5^\circ$ -resolution climate dataset for the twentieth century (Mitchell 2005) coupled to a water-balance model. The joint variability of estimated global runoff and global SSTs is examined. The objective of this paper is to identify the primary modes of variability in global annual runoff and associated variability of global annual SSTs during the previous century.

## 2. Datasets

Monthly temperature and precipitation data for the globe were obtained from Climate Research United at East Anglia, United Kingdom [the CRUTS2.1 dataset (Mitchell 2005)]. This dataset includes monthly temperature and precipitation data on a  $0.5^\circ \times 0.5^\circ$  grid for the land areas of the globe and spans the period 1901 through 2002. These data were used as inputs to a monthly water-balance model to generate time series of annual runoff for each grid cell. In addition to temperature and precipitation data, soil moisture storage capacity on a  $0.5^\circ \times 0.5^\circ$  grid was used with the water-balance model (Patterson 1990; Milly 1994; Milly and Dunne 1994); these data were obtained from the Geophysical Fluid Dynamics Laboratory (Princeton, New Jersey).

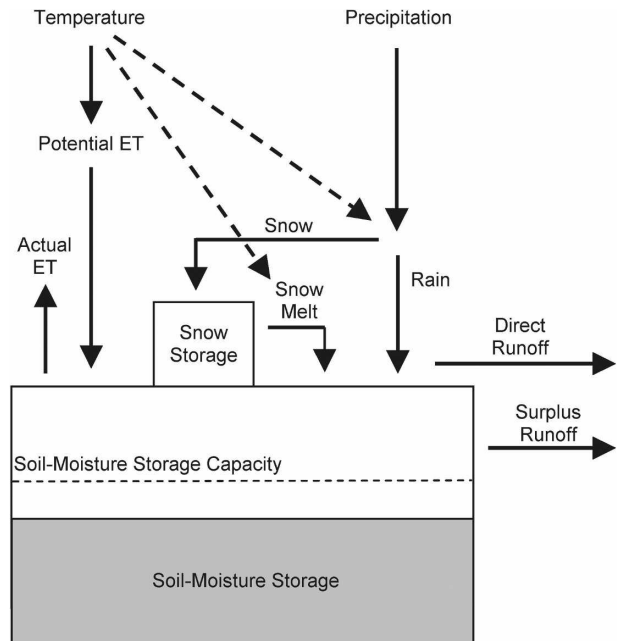


FIG. 1. Diagram of the water-balance model.

Monthly sea surface temperature data were obtained from the Kaplan extended dataset of monthly SSTs (Kaplan et al. 1998). The SST data are on a  $5^\circ \times 5^\circ$  grid and span the period 1856 to the present. The monthly SST data were aggregated to compute mean annual SSTs for the  $5^\circ \times 5^\circ$  grid.

## 3. The water-balance model

The water-balance model (Fig. 1) uses an accounting procedure to compute the allocation of water among various components of the hydrologic system (Thornthwaite 1948; Mather 1978, 1979; McCabe and Ayers 1989; McCabe and Wolock 1999; Wolock and McCabe 1999). The water-balance model includes the concepts of climatic water supply and demand, seasonality in climatic water supply and demand, snow accumulation and melt, and soil-moisture storage (Wolock and McCabe 1999; McCabe and Markstrom 2007). Climate inputs to the model are monthly precipitation and potential evapotranspiration, which is calculated from monthly temperature using the Hamon equation (Hamon 1961). In the water-balance model, when precipitation for a month is less than potential evapotranspiration, actual evapotranspiration is equal to precipitation plus the amount of moisture that can be removed from the soil. The fraction of soil-moisture storage that can be removed decreases linearly with decreasing soil-moisture storage; that is, water becomes more difficult

to remove from the soil as the soil becomes drier and less moisture is available for actual evapotranspiration. When precipitation exceeds potential evapotranspiration in a given month, actual evapotranspiration is equal to potential evapotranspiration; water in excess of potential evapotranspiration replenishes soil-moisture storage. When soil-moisture storage reaches capacity during a given month, the excess water becomes surplus. In a given month, 50% of the total surplus becomes runoff; the remaining surplus is carried over to the following month. The water-balance model also accounts for the accumulation and melt of snow in cold regions. Snow that melts becomes available to recharge soil moisture storage and/or to become surplus and, ultimately, runoff.

For details of the water-balance model, see McCabe and Markstrom (2007). The water-balance model was not calibrated; rather, standard parameter values were used (see McCabe and Markstrom 2007). Similar water-balance models were used by Legates and Mather (1992) and Legates and McCabe (2005) to compute mean-annual global runoff.

#### 4. Simulations and data aggregation

The water balance was run for each of the 50 173 grid cells from the CRUTS2.1 dataset between 60°N and 60°S latitude. CRUTS2.1 data poleward of these latitudes were not used in the analysis because many of the monthly temperature and precipitation values for these grid cells were generated from very sparse data. The monthly runoff values generated for each grid cell were subsequently summed to produce time series of annual runoff for the period 1905–2002. Although the CRUTS2.1 dataset begins in 1901, the first few years of the water-balance simulations were not analyzed, so that the effects of prescribed initial conditions would be minimized. In addition, for computational efficiency, the 50 173 time series of annual runoff were aggregated to a 5° latitude × 5° longitude grid, resulting in 638 grid cells (Fig. 2a), each with a unique time series. The time series values for the 5° × 5° grid were used in subsequent analyses.

The native SST data also were on a 5° × 5° grid and included 1207 grid cells with complete data for 1905–2002. The selection of grid cells with complete data for the study period excluded some cells, particularly in the Southern Hemisphere. The 5° × 5° SST grid cells were resampled (i.e., every other grid cell was chosen for analysis for the area between 60°N and 60°S latitude) to provide a similar number of SST grid cells as the runoff data. The resampling of the SST data provided 580 SST grid cells for analysis (Fig. 2b).

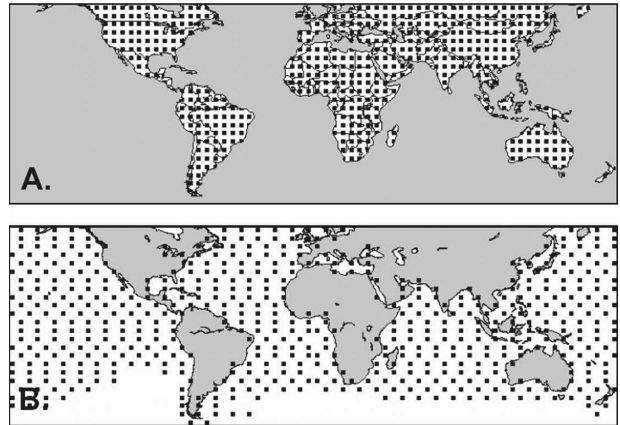


FIG. 2. Grids used for the (a) global annual runoff and (b) SST data.

#### 5. Water-balance model accuracy

The runoff estimates from the water-balance model were compared to time series of measured runoff for 18 drainage basins across the globe (Fig. 3; Table 1). These drainage basins include a range of physiographic regions. Monthly data for the Columbia and Mississippi Rivers were obtained from the U.S. Geological Survey (<http://waterdata.usgs.gov/nwis/sw>); data for all other basins were obtained from the Global River Discharge Database (<http://www.sage.wisc.edu/riverdata>). Monthly streamflow data are available from these sites, and the streamflow data were converted to monthly runoff values by dividing by the respective drainage basin areas. The monthly data then were summed to provide time series of measured annual runoff. The measured annual runoff values for these basins were compared with water-balance estimates that were aggregated for each of these basins. The water-balance estimates were aggregated from the 0.5°-resolution data (50 173 grid cells) rather than the 5° gridded data.

Errors in water-balance estimated runoff are a result of model error, as well as errors and limitations in observations of precipitation and temperature. In this study, temporal variability is the focus of the analysis; thus, the time series of measured and water-balance estimated runoff were standardized to remove any bias in water-balance estimated runoff while preserving the relative year-to-year variability. Values in each time series of runoff data were standardized by subtracting the respective long-term mean from each value in the time series and then dividing each departure by the respective long-term standard deviation. Transformation into standardized departures causes each runoff time series to have a mean of zero and a variance of one. The time series of SST data also were standardized prior to analysis.

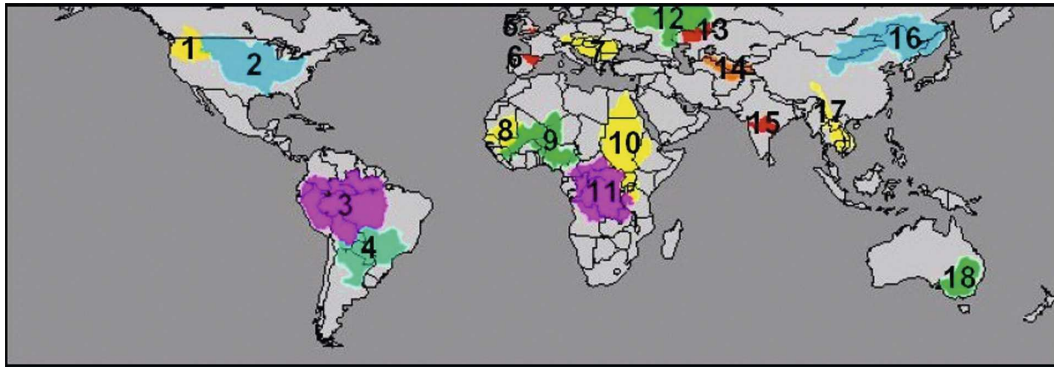


FIG. 3. Location of drainage basins used for the water-balance model verification. The numbers in the figure refer to the list in Table 1.

Table 1 presents Pearson correlation coefficient ( $R$ ) values between time series of standardized departures of measured and water-balance estimated runoff for the 18 basins. All of the  $R$  values are statistically significant at a 95% confidence level. The minimum, median, and maximum  $R$  values among the basins are 0.56, 0.76, and 0.96, respectively. Although the lowest  $R$  values are for basins in Europe and Asia, these regions also contained basins with higher  $R$  values. The lack of reliable temperature and precipitation time series for some areas may have contributed to errors in model estimates.

TABLE 1. List of stream gauges used to verify the water-balance model runoff estimates and correlations between measured and water-balance estimated annual runoff. The numbers along the left-hand side of the table refer to the numbers in Fig. 3. All of the correlations ( $R$ ) between measured and water-balance estimated annual runoff are statistically significant at a 95% confidence level, and, except for the Mekong at Mukdahan, the correlations are significant at a 99% confidence level.

Stream gauge	Period	Years	$R$
1. Columbia at The Dalles	1905–2002	98	0.85
2. Mississippi at Vicksburg	1932–88	57	0.86
3. Amazon at Obidos	1970–95	26	0.77
4. Parana at Corrientes	1969–79	11	0.78
5. Thames at Teddington	1965–84	20	0.73
6. Ebro at Tortosa	1913–62	50	0.79
7. Danube at Bezdan	1950–84	35	0.65
8. Senegal at Bakel	1951–84	34	0.96
9. Niger at Koulikoro	1908–90	83	0.80
10. Nile at Aswan	1912–64	53	0.76
11. Zaier at Kinshasa	1905–83	79	0.70
12. Volga at Volgograd	1905–35	31	0.82
13. Ural at Kushum	1921–84	64	0.58
14. Amu-Darya at Chatly	1938–73	36	0.71
15. Godavari at Polavaram	1912–60	49	0.85
16. Amur at Komsomolsk	1933–84	47	0.80
17. Mekong at Mukdahan	1950–86	36	0.56
18. Murray at Lock 9	1973–84	12	0.76

Some of the error also may be due to the simplicity of the water-balance model; natural hydrological processes that are important in some regions may not be represented well in the model. In addition, the model does not consider manmade factors, such as water storage and management, which would be expected to have a significant effect in some basins. Overall, however, the level of agreement between the water-balance model and measured flow at the test sites is considered adequate for the objectives of this study.

## 6. Runoff and sea surface temperature variability

The gridded standardized runoff and SST data were combined into one dataset by treating the time series (runoff or SST) at each grid cell as an individual variable. Thus, the combined dataset included 1218 variables (638 runoff grid cells and 580 SST grid cells). Each of the 1218 variables had 98 values, one value for each year in the time series (1905–2002).

Temporal variability of the combined annual runoff and sea surface temperature data was examined by using principal components analysis (PCA). The PCA of the combined global annual runoff and global annual SST data resulted in three principal components (PC1, PC2, and PC3) that explain 29% of the variance in the combined runoff and SST data (Table 2). The first component explains 15%, the second 9%, and the third 5% of the total variance. Subsequent components each explain less than 4% of the total variance.

The PCA of the combined runoff and SST data also was evaluated in terms of the relative amount of variance explained in the runoff and SST datasets individually (Table 2). The first three components from the PCA explain approximately 12% of the variance in the runoff data and 49% of the variance in the SST data. The amount of runoff variance explained by the PCs is

TABLE 2. Percent explained variance for PC1, PC2, and PC3 from a principal components analysis of global annual runoff and SSTs, 1905–2002.

	Runoff and SST data	Runoff data only	SST data only
PC1	15	4	27
PC2	9	4	15
PC3	5	4	7
Total	29	12	49

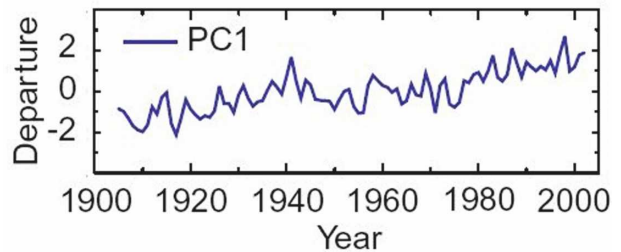
small because of the large amount of random variability (i.e., noise) in the runoff data. In contrast, the SST data exhibit a great deal of spatial and temporal autocorrelation and, therefore, a large amount of variance is explained by the retained PCs. The amount of variance explained in the runoff data by the PCs, although small, is consistent with previous studies of global hydroclimatic data. For example, Dai et al. (1997) reported two principal components that explained 11% of global precipitation and Dai et al. (2004) identified two principal components that explained nearly 12% of global PDSI data.

An additional analysis was performed to verify the results of the PCA. This analysis involved a singular value decomposition of the joint runoff and SST datasets. Singular value decomposition isolates dominant modes of cross covariance between datasets (Enfield and Alfaro 1999) and has been used in a number of climatic studies (Enfield and Alfaro 1999; McCabe and Palecki 2006). An SVD of the global annual runoff and SST data used in the current study produced similar results (not shown) to that of the joint PCA. The first three SVD expansion coefficients explained 30% of the total variance in the runoff and SST data (explaining 14% of the variance in the runoff data and 49% of the variance in the SST data). These values are similar to the variance explained by the joint PCA (Table 2). In addition, the corresponding PCA score and SVD expansion coefficient time series are highly correlated, with correlation coefficient values ranging from 0.83 to 0.98.

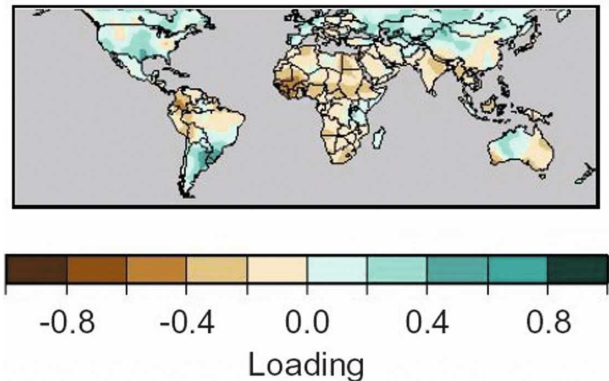
#### a. Component 1 of the combined runoff/SST dataset

The time series of the first principal component (PC1) scores indicates a long-term trend in the data (Fig. 4a). Because the signs of principal component scores are arbitrary, an examination of correlations (i.e., loadings) between the PC score time series and the input data time series (i.e., runoff and SSTs) is necessary to interpret the results. In the analysis presented here, positive (negative) runoff loadings are indicative

#### A. PC1 Scores



#### B. PC1 Runoff Loadings



#### C. PC1 SST Loadings

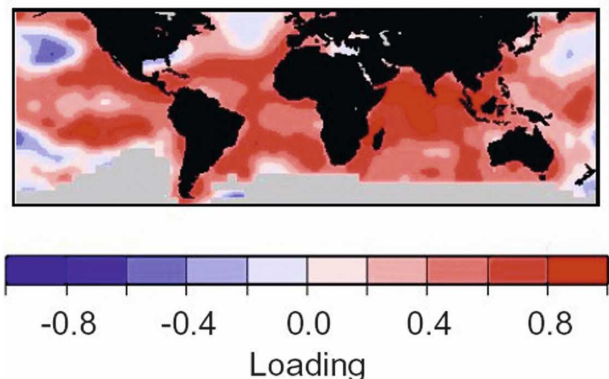


FIG. 4. (a) Score time series for PC1 from a PCA of combined global annual runoff and global annual SSTs, 1905–2002. (b) Runoff loadings for PC1. (c) SST loadings for PC1.

of increases (decreases) in runoff. The runoff loadings for PC1 indicate positive values (i.e., upward trends) in runoff for parts of North and South America, a large part of Asia, and Australia (Fig. 4b). These upward trends in runoff are consistent with the upward trends in global precipitation reported by Dai et al. (1997). Substantial negative loadings (i.e., downward trends) in runoff primarily are found for western Africa.

Linear trends, determined using simple correlations with time, were calculated for each runoff and SST grid cell. The correlation between the spatial pattern of runoff loadings for PC1 and the spatial pattern of linear trends in runoff for every runoff grid cell is 0.80 ( $p < 0.01$ ). Overall, only 169 (26%) of the  $5^\circ \times 5^\circ$  grid cells indicate any significant ( $p < 0.05$ ) trend in runoff; 117 (18%) grid cells show upward trends and 52 (8%) indicate downward trends. The upward trends are primarily in high-latitude locations and downward trends are primarily in low latitudes, particularly western Africa. This pattern of trends in runoff is similar to runoff trends projected by general circulation models (Dai et al. 1997; Nijssen et al. 2000) for climatic conditions associated with global warming. The pattern of runoff trends also is consistent with an observed shift in storm tracks to higher latitudes (McCabe et al. 2001); another expected result of global warming. As global temperatures have increased, storm tracks have moved poleward resulting in a poleward shift of precipitation and thus runoff.

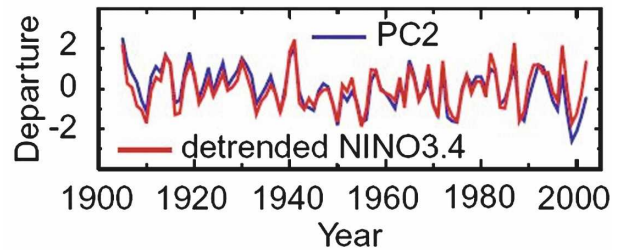
In addition, the trends in runoff are strongly associated with trends in precipitation rather than with trends in temperature. The correlations between the pattern of trends in runoff and the pattern of trends in precipitation and temperature are 0.92 ( $p < 0.01$ ) and  $-0.11$  (nonsignificant), respectively.

The spatial pattern of SST loadings for PC1 (Fig. 4c) shows increasing SSTs for most of the oceans. The correlation between the spatial patterns of SST loadings for PC1 and linear trends for every SST grid cell is 0.80 ( $p < 0.01$ ). The loading values for SSTs are generally larger than the runoff loading values. This is related to the lower runoff variance explained by the PCs compared with the SST variance explained (Table 2).

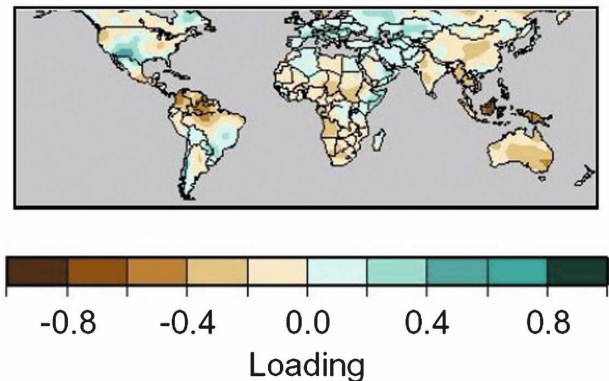
#### b. Component 2 of the combined runoff/SST dataset

The pattern of runoff and SST loadings for PC2 (Fig. 5) indicates that this component is representative of the association of ENSO with global annual runoff and SSTs. For example, the northwestern/southwestern U.S. dipole is apparent (Redmond and Koch 1991) as well as the ENSO signal in South America and Australia (Dettinger et al. 2000; Dettinger and Diaz 2000). The pattern indicated by the PC2 loadings is similar to the relations between the Southern Oscillation index and streamflow presented by Dettinger and Diaz (2000). The pattern illustrated in Fig. 5b is most likely forced by precipitation anomalies related with ENSO (Ropelewski and Halpert 1987; Dai and Wigley 2000; Trenberth and Caron 2000; Dai et al. 2004). Dai et al. (1997, 2004) also found that one of the primary modes

#### A. PC2 Scores



#### B. PC2 Runoff Loadings



#### C. PC2 SST Loadings

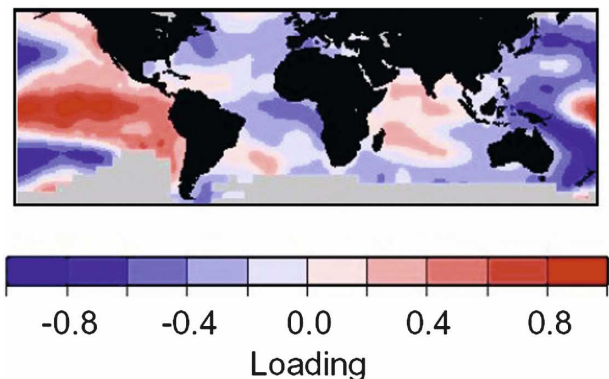


FIG. 5. (a) Score time series for PC2 from a PCA of combined global annual runoff and global annual SSTs, 1905–2002; also plotted are detrended Niño-3.4 SSTs. (b) Runoff loadings for PC2. (c) SST loadings for PC2.

of global precipitation and global PDSI variability was related to ENSO.

The SST loadings for PC2 indicate large positive loadings in the tropical Pacific Ocean, where the ENSO signal primarily occurs. A comparison of a time series of detrended Niño-3.4 ( $5^\circ\text{N}$ – $5^\circ\text{S}$ ,  $170^\circ$ – $120^\circ\text{W}$ ) SSTs

with the score time series for PC2 (Fig. 5a) indicates a significant correlation [correlation coefficient equal to 0.85 ( $p < 0.01$ )]. The Niño-3.4 time series was detrended for this comparison because the long-term trend in the runoff and SST data is represented by PC1 and therefore should not be evident in subsequent PCs. (The Niño-3.4 time series data were obtained from <http://climexp.knmi.nl/data/inino5.dat>.)

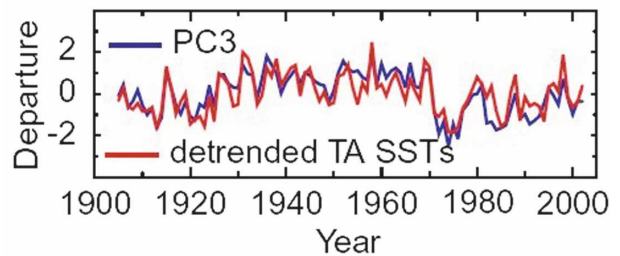
### c. Component 3 of the combined runoff/SST dataset

The SST loadings pattern for PC3 (Fig. 6) indicates that the strongest signal is in the North Atlantic Ocean, particularly the tropical North Atlantic Ocean. These correlations suggest an association between variability in tropical North Atlantic SSTs and annual runoff for some regions. Comparison of a time series of detrended tropical North Atlantic SSTs (computed as the average of annual SSTs for the region from 5°N to 20°N and from 60°W to 20°W) with the score time series for PC3 indicates a correlation of 0.81 ( $p < 0.01$ ; Fig. 6a).

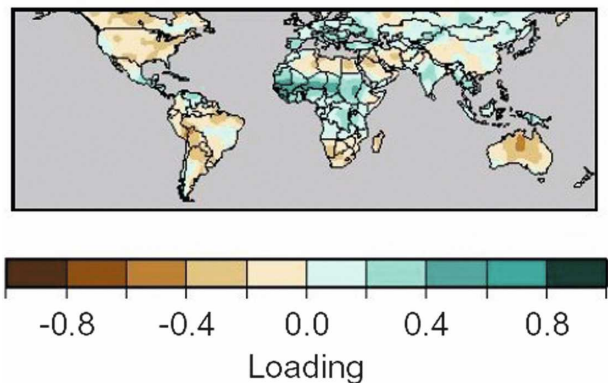
These results are consistent with previous research that has suggested an association between variability of North Atlantic SSTs and global climate (Enfield et al. 2001; McCabe et al. 2004; Sutton and Hodson 2005; McCabe and Palecki 2006; Sutton and Hodson 2007). There have been a number of findings in the literature identifying influences of changes in Atlantic SSTs on drought and precipitation variations in Canada (Shabbar and Skinner 2004), Africa (Fontaine and Janicot 1996; Jury 2003), Europe (Rodwell et al. 1999), South America (Carton et al. 1996), and the Caribbean (Gianini et al. 2003). In a recent modeling study, Sutton and Hodson (2007) suggest that the influence of the tropical North Atlantic on global hydroclimate may be larger than the influence of the mid- to high-latitude North Atlantic.

The runoff loadings pattern for PC3 (Fig. 6b) is consistent with previously noted associations between North Atlantic SSTs and global PDSI values (McCabe and Palecki, 2006). Negative loadings dominate North America, most of South America, and Australia. Positive loadings are found over western and central Africa, most of Europe, and much of Asia. Previous studies have indicated that the North Atlantic SST associations with global hydroclimate are particularly noticeable on decadal to multidecadal time scales (Enfield et al. 2001, McCabe et al. 2004, McCabe and Palecki 2006; Sutton and Hodson 2007). A comparison of 10-yr moving averaged PC3 scores and 10-yr moving averaged and detrended tropical North Atlantic SSTs indicates a substantial association between decadal to multidecadal

### A. PC3 Scores



### B. PC3 Runoff Loadings



### C. PC3 SST Loadings

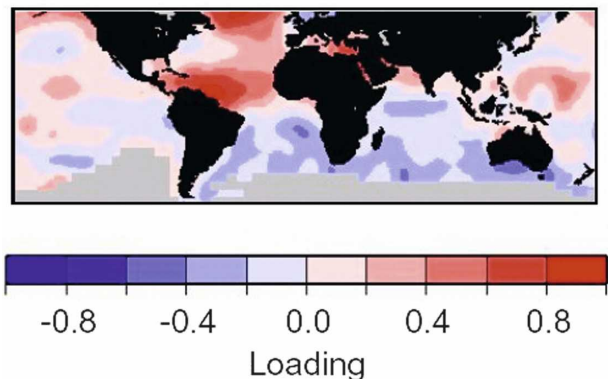


FIG. 6. (a) Score time series PC3 from a PCA of combined global annual runoff and global annual SSTs, 1905–2002; also plotted are detrended tropical North Atlantic SSTs (TA SSTs). (b) Runoff loadings for PC3. (c) SST loadings for PC3.

regimes of PC3 and tropical North Atlantic SSTs [correlation coefficient equal to 0.91 ( $p < 0.01$ )].

An interesting feature of the PC3 score time series (Fig. 6a) is an abrupt change (or shift) to negative values around 1970. This abrupt shift also is apparent in the time series of tropical North Atlantic SSTs and has been noted in other records. For example, McCabe and

Wolock (2002) found an apparent steplike increase in runoff and precipitation in the eastern United States that occurred around 1970. The shift also is evident in runoff data for western Africa and Australia (data not shown). These results suggest that the steplike change in runoff may be related to a shift in tropical North Atlantic SSTs around 1970.

Although the physical mechanisms that explain the associations between North Atlantic SSTs and global climate are still unknown, this is an area of active research (e.g., Lu and Dong 2005; Sutton and Hodson 2007; Zhang and Delworth 2006; Zhang et al. 2007). Some proposed physical processes include a northward expansion of the Hadley cell (Seager et al. 2007), effects on Atlantic hurricane development (Zhang and Delworth 2006), and interactions with Pacific SSTs (Dong et al. 2006; Lu and Dong 2005; Seager et al. 2005).

## 7. Conclusions

The analysis of global runoff and SST data identified three modes of variability. The first mode of variability reflects a long-term trend in runoff and SSTs, the second mode reflects ENSO variability, and the third mode represents associations between variability of tropical North Atlantic SSTs and annual runoff for some regions.

The trends in global annual runoff generally indicate that annual runoff has been increasing in the mid- to high latitudes and decreasing in the low latitudes. While consistent with theories of global climate change due to increasing greenhouse gases in the atmosphere, alternative hypotheses also should be considered. For example, some researchers (Friis-Christensen and Lassen 1991; Lassen and Friis-Christensen 1995) have suggested that twentieth-century warming is due to variability in solar output. In addition, Cohn and Lins (2005) have pointed out that apparent hydroclimatic trends can be caused by long-term persistence in random processes. This makes the assignment of cause and effect in the analysis of time series data problematic.

Results also suggest that SSTs in the tropical North Atlantic Ocean may be a source of hydroclimatic variability that requires additional research. Hydroclimatic effects of variability in tropical North Atlantic SSTs may be especially important on decadal to multidecadal time scales.

## REFERENCES

- Carton, J. A., X. Cao, B. S. Giese, and A. M. Da Silva, 1996: Decadal and interannual SST variability in the tropical Atlantic Ocean. *J. Phys. Oceanogr.*, **26**, 1165–1175.
- Cohn, T. A., and H. F. Lins, 2005: Nature's style: Naturally trendy. *Geophys. Res. Lett.*, **32**, L23402, doi:10.1029/2005GL024476.
- Dai, A. G., and T. M. L. Wigley, 2000: Global patterns of ENSO-induced precipitation. *Geophys. Res. Lett.*, **27**, 1283–1286.
- Dai, A., I. Y. Fung, and A. D. Del Genio, 1997: Surface observed global land precipitation variations during 1900–88. *J. Climate*, **10**, 2943–2962.
- , K. E. Trenberth, and T. Qian, 2004: A global dataset of Palmer Drought Severity Index for 1870–2002: Relationship with soil moisture and effects of surface warming. *J. Hydrometeorol.*, **5**, 1117–1130.
- Dettinger, M. D., and H. F. Diaz, 2000: Global characteristics of streamflow seasonality and variability. *J. Hydrometeorol.*, **1**, 289–310.
- , D. R. Cayan, G. J. McCabe, and J. A. Marengo, 2000: Multiscale streamflow variability associated with El Niño/Southern Oscillation. *El Niño and the Southern Oscillation: Multiscale Variability and Global and Regional Impacts*, H.F. Diaz and V. Markgraf, Eds., Cambridge University Press, 496 pp.
- Dong, B., R. T. Sutton, and A. A. Scaife, 2006: Multidecadal modulation of El Niño–Southern Oscillation (ENSO) variance by Atlantic Ocean sea surface temperatures. *Geophys. Res. Lett.*, **33**, L08705, doi:10.1029/2006GL025766.
- Enfield, D. B., and E. T. Alfaro, 1999: The dependence of Caribbean rainfall on the interaction of the tropical Atlantic and Pacific Oceans. *J. Climate*, **12**, 2093–2103.
- , A. M. Mestas-Nunez, and P. J. Trimble, 2001: The Atlantic multidecadal oscillation and its relation to rainfall and river flows in the continental U.S. *Geophys. Res. Lett.*, **28**, 2077–2080.
- Fontaine, B., and S. Janicot, 1996: Sea surface temperature fields associated with West African rainfall anomaly types. *J. Climate*, **9**, 2935–2940.
- Friis-Christensen, E., and K. Lassen, 1991: Length of the solar cycle: An indicator of solar activity closely associated with climate. *Science*, **254**, 698–700.
- Giannini, A., R. Saravanan, and P. Chang, 2003: Oceanic forcing of Sahel rainfall on interannual and interdecadal time scales. *Science*, **302**, 1027–1030.
- Gray, S. T., J. L. Betancourt, C. L. Fastie, and S. T. Jackson, 2003: Patterns and sources of multidecadal oscillations in drought-sensitive tree-ring records from the central and southern Rocky Mountains. *Geophys. Res. Lett.*, **30**, 1316, doi:10.1029/2002GL016154.
- Hamon, W. R., 1961: Estimating potential evapotranspiration. *J. Hydraul. Div. Amer. Soc. Civ. Eng.*, **87**, 107–120.
- Hidalgo, H. G., 2004: Climate precursors of multidecadal drought variability in the western United States. *Water Resour. Res.*, **40**, W12504, doi:10.1029/2004WR003350.
- Jury, M. R., 2003: The coherent variability of African river flows: Composite climate structure and the Atlantic circulation. *Water SA*, **29**, 1–10.
- Kaplan, A., M. Cane, Y. Kushnir, A. Clement, M. Blumenthal, and B. Rajagopalan, 1998: Analyses of global sea surface temperature 1856–1991. *J. Geophys. Res.*, **103**, 18 567–18 589.
- Lassen, K., and E. Friis-Christensen, 1995: Variability of the solar cycle length during the past five centuries and the apparent association with terrestrial climate. *J. Atmos. Terr. Phys.*, **57**, 835–845.
- Legates, D. R., and J. R. Mather, 1992: An evaluation of the average annual global water balance. *Geogr. Rev.*, **82**, 253–267.

- , and G. J. McCabe, 2005: A re-evaluation of the average annual global water balance. *Phys. Geogr.*, **26**, 467–479.
- Lu, R., and B. Dong, 2005: Impact of Atlantic sea surface temperature anomalies on the summer climate in the western North Pacific during 1997–1998. *J. Geophys. Res.*, **110**, D16102, doi:10.1029/2004JD005676.
- Mather, J. R., 1978: *The Climatic Water Balance in Environmental Analysis*. D.C. Heath, 239 pp.
- , 1979: Use of the climatic water budget to estimate streamflow. *Publ. Climatol.*, **32**, 1–52.
- McCabe, G. J., and M. A. Ayers, 1989: Hydrologic effects of climate change in the Delaware River Basin. *Water Resour. Bull.*, **25**, 1231–1242.
- , and D. M. Wolock, 1999: Future snowpack conditions in the western United States derived from general circulation model climate simulations. *J. Amer. Water Resour. Assoc.*, **35**, 1473–1484.
- , and —, 2002: A step increase in streamflow in the conterminous United States. *Geophys. Res. Lett.*, **29**, 2185, doi:10.1029/2002GL015999.
- , and M. A. Palecki, 2006: Multidecadal climate variability of global lands and oceans. *Int. J. Climatol.*, **26**, 849–865.
- , and S. L. Markstrom, 2007: A monthly water-balance model driven by a graphical user interface. U.S. Geological Survey Open-File Rep. 2007-1088, 6 pp.
- , M. P. Clark, and M. C. Serreze, 2001: Trends in Northern Hemisphere surface cyclone frequency and intensity. *J. Climate*, **14**, 2763–2768.
- , M. A. Palecki, and J. L. Betancourt, 2004: Pacific and Atlantic Ocean influences on multidecadal drought frequency in the United States. *Proc. Natl. Acad. Sci. USA*, **101**, 4137–4141.
- Milly, P. C. D., 1994: Climate, soil water storage, and the average annual water balance. *Water Resour. Res.*, **30**, 2143–2156.
- , and K. A. Dunne, 1994: Sensitivity of the global water cycle to the water-holding capacity of land. *J. Climate*, **7**, 506–526.
- Mitchell, T. D., 2005: An improved method of constructing a database of monthly climate observations and associated high resolution grids. *Int. J. Climatol.*, **25**, 693–712.
- Nicholson, S. E., D. Leposo, and J. Grist, 2001: The relationship between El Niño and drought over Botswana. *J. Climate*, **14**, 323–335.
- Nijssen, B., G. M. O'Donnell, A. Hamlet, and D. P. Lettenmaier, 2000: Hydrologic sensitivity of global rivers to climate change. *Climatic Change*, **50**, 515–517.
- Parker, D., C. Folland, A. Scaife, J. Knight, A. Colman, P. Baines, and B. Dong, 2007: Decadal to multidecadal variability and the climate change background. *J. Geophys. Res.*, **112**, D18115, doi:10.1029/2007JD008411.
- Patterson, K., 1990: Global distributions of total and total-available soil water-holding capacities. M.S. thesis, Department of Geography, University of Delaware, 119 pp.
- Redmond, K. T., and R. W. Koch, 1991: Surface climate and streamflow variability in the western United States and their relationship to large-scale circulation indices. *Water Resour. Res.*, **27**, 2381–2399.
- Rodwell, M. J., D. P. Rowell, and C. K. Folland, 1999: Oceanic forcing of the wintertime North Atlantic Oscillation and European climate. *Nature*, **398**, 320–323.
- Ropelewski, C. F., and M. S. Halpert, 1987: Global and regional scale precipitation patterns associated with the El Niño/Southern Oscillation. *Mon. Wea. Rev.*, **115**, 1606–1626.
- Schubert, S. D., M. J. Suarez, P. J. Pegion, R. D. Koster, and J. T. Bacmeister, 2004: On the cause of the 1930s Dust Bowl. *Science*, **303**, 1855–1859.
- Seager, R., Y. Kushnir, C. Herweijer, N. Naik, and J. Velez, 2005: Modeling of tropical forcing of persistent droughts and pluvials over western North America: 1856–2000. *J. Climate*, **18**, 4068–4091.
- , and Coauthors, 2007: Model projections of an imminent transition to a more arid climate in southwestern North America. *Science*, **316**, 1181–1184, doi:10.1126/science.1139601.
- Shabbar, A., and W. Skinner, 2004: Summer drought patterns in Canada and the relationship to global sea surface temperatures. *J. Climate*, **17**, 2866–2880.
- Sutton, R. T., and D. L. R. Hodson, 2003: Influence of the ocean on North Atlantic climate variability 1871–1999. *J. Climate*, **16**, 3296–3313.
- , and —, 2005: Atlantic Ocean forcing of multidecadal variations in North American and European summer climate. *Science*, **309**, 115–118.
- , and —, 2007: Climate response to basin-scale warming and cooling of the North Atlantic Ocean. *J. Climate*, **20**, 891–907.
- Thornthwaite, C. W., 1948: An approach toward a rational classification of climate. *Geogr. Rev.*, **38**, 55–94.
- Trenberth, K. E., and J. M. Caron, 2000: The Southern Oscillation revisited: Sea level pressures, surface temperatures, and precipitation. *J. Climate*, **13**, 4358–4365.
- Wolock, D. M., and G. J. McCabe, 1999: Effects of potential climatic change on annual runoff in the conterminous United States. *J. Amer. Water Resour. Assoc.*, **35**, 1341–1350.
- Zhang, R., and T. L. Delworth, 2006: Impact of Atlantic multidecadal oscillations on India/Sahel rainfall and Atlantic hurricanes. *Geophys. Res. Lett.*, **33**, L17712, doi:10.1029/2006GL026267.
- , —, and I. M. Held, 2007: Can the Atlantic Ocean drive the observed multidecadal variability in Northern Hemisphere mean temperature? *Geophys. Res. Lett.*, **34**, L02709, doi:10.1029/2006GL028683.